AD-A082 229 STEVENS INST OF TECH HOBOKEN N J DEPT OF PHYSICS F/G 20/9
STUDY OF THE ANATOMY OF THE X-RAY AND NEUTRON PRODUCTION SCALIN--ETC(U)
DEC 78 V NARDI, W H BOSTICK, W PRIOR AFOSR-75-2754
UNCLASSIFIED SIT-P2001-1278 AFOSR-TR-80-0224 NL

1 OF 1
AD
A082229

END
DATE FILMED
4-80
DTIC

SIT

DEPARTM
OF PHY

Study of the Anatom
X-Ray and Neutron Pr
Scaling Laws in the Pl
(Particle Energy S

V. Nardi, W. H. Bostic

Annual Report AFOSR Gr
Period Oct. 1, 1977 - Se

December 1

A

Appr
distr

80

UNCLASSIFIED
CLASSIFICATION OF THIS PAGE (When Data Entered)

REPORT DOCUMENTATION PAGE	READ INSTRUCTIONS BEFORE COMPLETING FORM
1. REPORT NUMBER **AFOSR-TR- 80-0224** 2. GOVT ACCESSION NO.	3. RECIPIENT'S CATALOG NUMBER
4. TITLE (and Subtitle) STUDY OF THE ANATOMY OF THE X-RAY AND NEUTRON PRODUCTION SCALING LAWS IN THE PLASMA FOCUS (PARTICLE ENERGY SPECTRUM)	5. TYPE OF REPORT & PERIOD COVERED Interim Technical Report Oct. 1, 1977 - Sept. 30, 1978 6. PERFORMING ORG. REPORT NUMBER SIT-P 2001-1278
7. AUTHOR(s) V. Nardi, W. H. Bostick, W. Prior	8. CONTRACT OR GRANT NUMBER(s) AFOSR-75-2754
9. PERFORMING ORGANIZATION NAME AND ADDRESS Stevens Institute of Technology Physics/Engineering Physics Department Castle Point Station, Hoboken, N.J. 07030	10. PROGRAM ELEMENT, PROJECT, TASK AREA & WORK UNIT NUMBERS 61102F 2301/A2
11. CONTROLLING OFFICE NAME AND ADDRESS Department of the Air Force, Air Force Office of Scientific Res., Directorate of Physics, Bldg. 410 Bolling Air Force Base, D 20332	12. REPORT DATE Dec. 1978 13. NUMBER OF PAGES 19
14. MONITORING AGENCY NAME & ADDRESS(if different from Controlling Office)	15. SECURITY CLASS. (of this report) unclassified 15a. DECLASSIFICATION/DOWNGRADING SCHEDULE

16. DISTRIBUTION STATEMENT (of this Report)

Approved for public release; distribution unlimited.

17. DISTRIBUTION STATEMENT (of the abstract entered in Block 20, if different from Report)

18. SUPPLEMENTARY NOTES

To be published with variation and with additional material in "Plasma Physics and Controlled Fusion Research", (Proc. Innsbruck International Conf., 1978) by the International Atomic Energy Agency, Vienna, Austria.

19. KEY WORDS (Continue on reverse side if necessary and identify by block number)

Neutron yield, x-ray emission, electron beams, ion beams, energy spectrum, terawatt ions and electron beams, correlation coefficients, beam-induced damage, high-intensity ion and electron beams, dendrites, plasma focus.

20. ABSTRACT (Continue on reverse side if necessary and identify by block number)

We use plasma focus discharges to generate high-intensity dueteron beams ($\sim 10^5$ Amp) with a $\gtrsim$ 300-keV-peaked spectrum and electron beams, with an energy distribution similarly peaked at 300-400 keV. The energy spectrum is determined by two independent methods (time of flight and target-damage data). The spectrum various from shot to shot but the main features are observed in all discharges. In each discharge we observe on a time interval of 100-300 nanosec a sequence of beam pulses (1-10), with the same multiplicity

DD FORM 1 JAN 73 1473 EDITION OF 1 NOV 65 IS OBSOLETE S/N 0102-LF-014-6601

UNCLASSIFIED
SECURITY CLASSIFICATION OF THIS PAGE (When Data Entered)

ABSTRACT

of the peaks in the electrode-current variations, ~~dI/dt~~. Correlation coefficients between x-ray and neutron yield in D_2 discharges and beam parameters have been determined by a variety of conditions for the PF (bank voltage, filling pressure, circuit inductance). The power level of both ions and electron beams is ~ 0.1-1 TW/cm^2.

1 Feb. 1979

Corrections

Annual Report AFOSR Grant 75-2754
Period Oct. 1, 1977-Sept. 30, 1978

Stevens Institute of Technology, Report SIT - P2001-1278
"Study of the Anatomy of the X-Ray and Neutron Production Scaling Laws in the Plasma Focus" (Particle Energy Spectrum)

Page	Line	Incorrect	Correct
4	3 (from above)	see Fig. 5	see Fig. 1
4	8 (from above)	see Fig. 6	see Fig. 2
6	7 (from above)	see Fig. 6	see Fig. 2
8	3 (from above)	Fig. 5	Fig. 1
8	8 (from above)	Fig. 6	Fig. 3
8	9 (from above)	Fig. 6 (a,b)	Fig. 3
8	7 (from below)	Fig. 5	Fig. 1
10	6 (from above)	Fig. 7	Fig. 4

Annual Scientific Report on AFOSR Grant 75-2754 for Period October 1, 1977 through September 30, 1978

1. Publications

A variety of methods and of diagnostic techniques have been developed and extensively used at Stevens Institute to correlate neutron and x-ray yield in plasma focus discharges with the energy spectrum of ion beams and with energy and electric charge of electron beams which are generated in these discharges. The following papers have been completed as a result of this research period ending September 1978:

(1) Energy Spectra of Deuteron Beams and Electron Beams from Focused Discharges and Optimization Criteria, V. Nardi, W. H. Bostick, J. Feugeas, W. Prior, C. Cortese, Proc. IAEA Int. Conference on Plasma Physics and Controlled Nuclear Fusion Research, Innsbruck, 23-30 Aug. 1978, Vol. III; (2) Production of GW Electron and Ion Beams by Focused Discharges, W. H. Bostick, J. Feugeas, V. Nardi, W. Prior, C. Cortese, Proc. Energy Storage, Compression and Switching Int. Conf. (II), Venice, Dec. 5-8, 1978, Plenum Publ. New York; (3) Structure and Propagation of Electron Beams, V. Nardi, Proc. Energy Storage, Compression and Switching Int. Conf. 1978; (4) Collective Acceleration and Focussing of Fast Ion Bursts, J. Luce, W. H. Bostick, V. Nardi, Proc. Int. Conf. on Collective Methods of Acceleration, Univ. of California, Irvine, May 22-25, 1978, Harwood Academic Publ., London, p. 423-507; (5) Electron Beams and 10^5 Amp Deuteron Beams by Focused Discharges, W. H. Bostick, V. Nardi, W. Prior, Optic. Soc. of Am., Tech. Digest, Feb. 1978, San Diego, p. Th 21-25.

2. Summary of the Research Activity and Findings.

Deuteron beams ($\gtrsim 10^5$ Amp) with a 300-keV-peaked spectrum and electron beams are produced by localized sources ($\gtrsim$ 10 ns, $\gtrsim$ 1 mm) in focused discharges. The energy spectrum of the deuteron beam ejected from a localized source in plasma focus discharges (45-75 μF at 15-18 kV; $I_{max} \sim$ 0.5-0.8 MA) is derived by two independent methods (A) ion time of flight and (B) ion-induced damage on Aℓ plates. The ion spectrum varies from shot to shot but specific features are observed by all discharges. From method (A) the number of deuterons N(E) as a function of the ion energy E has a well defined maximum N_m for 130 keV $\leq E \leq$ 320 keV. N(E) has a minimum at lower values of E and rises sharply again by further decreasing E. N(E) for $E \lesssim$ 50 keV becomes substantially larger than N_m. N(E $\sim$ 1 MeV) can still be high as $\sim 0.1\ N_m$. The distribution of ion penetration range in Aℓ yields by method (B) substantially the same spectrum as method (A). A second peak with maximum value N_M of N(E) for 15 keV $\lesssim E \lesssim$ 40 keV is derived by (B) method which is most convenient for deriving the low-energy tail of the ion spectrum ($N_M \sim 9\ N_m$). A more detailed description of methods and findings is reported in References 1, 2, 3, 4, 5.

The electron-beam energy (with a dominant value $\gtrsim$ 300-400 keV) is determined by the length of dendrites ($\gtrsim$ penetration range) in a lucite target inserted inside the hollow center electrode (anode). The total neutron yield n in a discharge is higher, the higher the maximum value E_M of the observed ion energy. By comparing two low-voltage discharges higher values of E_M and n are observed in the discharge which generates fewer ion (and electron) beams. In a high voltage discharge n has instead higher values when the dischage generates many ion/electron beams. This part of our research activity is described in the following paragraphs and has been reported to some extend in our publication (1).

3. Energy and Total Charge of Electron Beams.

A disc of plexiglass (polymethylimethacrylate - PMMA) was used as a target for the electron beams which propagate along the anode axis (see Fig. 5). The disc $\sim$ 5 mm thick had the same diameter as the hollow center electrode (anode) and was fitted inside the anode at a distance > 10 cm from the anode end where electron beams are generated with a maximum of energy (disc surface orthogonal to the electrode axis). Dendrites are formed in the PMMA after exposure to a single plasma-focus discharge (see Fig. 6) as a consequence of the fact that electrons are stopped and trapped within the PMMA and a negative space charge builds up.PMMA breakdown occurs after or during the electron bombardment. The dendrites form the discharge pattern inside the PMMA (Lichtenberg figures) and indicate that the PMMA is ruptured through the irradiated volume (the disc surface on the side of the plasma is at the positive voltage). The PMMA breakdown and the formation of the discharge pattern are easily understood by assuming that the bulk of the space charge in the PMMA is localized in a relatively thin layer parallel to the exposed - or free - surface of the disc which is bombarded by the electron beam. Experiments by other laboratories provide the evidence of the high concentration of the space charge in a narrow layer in PMMA samples which had been irradiated by a monocromatic electron beam (6).

The distance δ between the charge layer and the free surface of the disc is given by the depth of the sharply defined region from which the dendrites originates.

An estimate of the energy E_e of the bulk of the electrons in the beam is immediately obtained by taking the electron penetration range $\lambda_e(E_e) \tilde{=} \delta$ (E_e vs. λ_e is taken from ref. 7). The true value of the electron energy is somewhat larger than the value of E_e as it is derived by this method because of the retarding field created by the charge build up in PMMA (the relative importance of retarding field and of collision losses in slowing down the electrons has been determined experimentally by other laboratories [8]). In Table I are reported the three typical values of δ which have been observed in a PMMA sample after exposure to a single PF discharge. The short duration of the electron beam ($\sim$ 100 ns) assures that charge-leakage effects before PMMA breakdown can be neglected.

We can define one component of the electron beam for each observed value of δ by characterizing a beam component by the corresponding value of E_e. The voltage due to charge accumulation in one of the three PMMA layer becomes large enough for breakdown on a time interval which cannot be expected to be the same for the three observed values of δ. It is justified by our experimental data to assume that the localized sources of the electron beams coincide in space and in time with the localized sources of the x-ray emission and that both have similar variations with time.

From the variations of the x-ray emission (3) we can consistently assume that the deposition in PMMA of the high-energy component of the beam ($E_e \gtrsim 300$ keV; see Table I) is completed earlier and on a shorter time interval than for the other two components; the low energy component ($\sim$ 50 keV) starts later and lasts longer than the other two components.

Under this assumption the breakdown of the PMMA slab from free surface to $\delta \tilde{=} 400$ μm can be considered as essentially independent from the breakdown processes of the two slabs with a smaller δ (these are considered to be mutually independent as well ; non-interference among the three breakdown processes is suggested also by the observation that the dendrites have a tree-like pattern with few twigs and do not extend to the whole slab volume see Fig. 6). In agreement with the previous assumption we can estimate the electric charge Q which is deposited in each one of the three thin layer inside the PMMA disc by using the formula for a planar capacitor with the dielectric breakdown strength of PMMA, i.e. $V_{br} \tilde{=} 5$ MV (m^{-1} on intrinsic breakdown mechanism is effective in our case)(9). The estimated values of Q and E_e are reported in Table I.

Table I

Data from Dendrites in PMMA (a disc located inside center electrode-anode).

Q (charge of thin layer inside PMMA) = CV_{br}

V_{br} (breakdown strength of PMMA at 100°C) ~ 5 MV cm^{-1}

$C = \frac{\epsilon A}{\delta}$ capacitance of dielectric slab of thickness δ and area A.

δ = observed distance between region from which dendrites originate and free surface of dielectric (ϵ = 2.5 dielectric constant of PMMA).

($\delta \lesssim$ mean forward electron range in PMMA)

A = area of damaged dielectric surface ~.01 cm^2 (depending on neutron yield).

Three typical values of δ have been observed (the PMMA disc is exposed to a single discharge).

$\delta(\mu m)$	$400 \pm 5\%$	100 - 140	15 - 20
E_e(keV)	300	130 - 140	44 - 52
Q(Coulomb)	2.5×10^{-4}	$10^{-3} - 7 \times 10^{-4}$	$6.5 \times 10^{-3} - 2 \times 10^{-3}$

4. Electron Beams

A pyrex pipe was attached at the rear end of the center electrode (Fig. 5) to serve as a drift chamber for the electron beams. A shielded Rogowski coil (RC) encircling the pyrex pipe was used to pick up the dI_e/dt signal due to electron beams. This RC was monitored simultaneously with the dI/dt signal from the total current on the electrodes. A second RC was used in many shots simultaneously with the first coil to have the integrated signal for I_e. The display of these signals from a Tektronix 7844 Oscilloscope are presented in Fig. 6.

The two Rogowski coils which give the signals in Fig. 6(a,b) are at a distance of $\tilde{\sim}$ 20 cm from the localized source of the electron beam (the coil location was changed in some discharges). A variety of tests have been made to check the noise level, the possibility of spurious signals and to verify that indeed the RC signal is generated by the electron beam current I_e. In one type of test, (A), the shielded RC was lifted at the side of the drift tube and the display sensitivity was increased several times. No signal was detected in this case. In another type of test, (B), the end of the anode near the focus was closed with a metal disc; also in this case the signal from the shielded RC, as in Fig. 5, was absolutely flat. This and the observed damage (a circular spot with area $\tilde{\sim}$ 0.1 cm^2) on a target at the end of the drift tube after a single shot prove that the RC signal is caused by the electron beam current I_e. The rise of I_e to peak value is very fast and in some shot is about 10 ns. The maximum observed value of I_e over about 50 shots was $\tilde{\sim}$ 5 kA. We can have that the actual value of I_e is substantially higher, by a factor 10-40, than the RC value because of the return current which is carried

by collectively-accelerated ions from the gas (6 torr D_2, or H_2, as in the discharge chamber) and/or by the polarization current on the wall of the chamber.[+] By using the value $I_e \gtrsim 5$ kA for a beam of electrons of 300 keV with a cross-sectional area $\gtrsim 0.1$ cm^2 we estimate a power of 15 Gw/cm^2 for this 15 J beam at the target. The hard x-ray signal from the beam-source region has a FWHM of 1-2 ns (scintillation detector signal). By taking this as the duration of the beam source the power at the source is 0.15 Tw/cm^2 or higher if the source diameter is smaller (this is certainly our case). A higher power value can be estimated by the energy deposition data from the target which is consistent with a value of I_e as corrected for return current effects. From Table I the energy carried by a beam can be as high as $\gtrsim$ 500 J, i.e. 10% of the energy of the capacitor bank. The power of the 300 keV component of the beam ($\gtrsim$ 100 J) which has the shortest duration at the RC distance from the source is then $\gtrsim$ 0.1 Terawatt/cm^2 and near the source the power then is at least 1 Tw/cm^2 or higher. These values coincide with the estimated power of the ion beam in the forward direction.

5. dI/dt data.

For each peak (or for each group of partially unresolved peaks), spanning $\sim$ 100-500 ns in the dI/dt signal (at the time of neutron emission onset) we have observed the emission of a sharply collimated electron beams which propagate along the axis of the hollow anode. In order to find a possible correlation among total neutron yield, multiplicity of electron beams and the details of the dI/dt signal we have analyzed the dI/dt signals of $\gtrsim$ 300 discharges with D_2 (6 Torr) filling with a 75 μF capacitor bank at different voltage values (12.5 - 18.5 kV).

[+]As well as by counterstreaming electrons which are produced (with the positive ions) by the primary-beam-induced ionization in the background gas.

An external inductance was attached to this system (PF-2) in order to have for $V \tilde{=} 16$ kV the same value of the peak current $I_o \tilde{=} 6 \times 10^5$A as in the 45 μF system (PF-1) that was used for the EB experiment reported in the previous section. The modified inductance of capacitor bank transmission line and electrodes of PF-2 was $L_o \tilde{=} 57$ nh i.e. twice the original value of L_o for usual PF-2 operation. In Fig. 7 is reported the mean value $\bar{n}$ of the neutron yield (n = neutrons/shot) over N shots with a specific value of the voltage V on the electrodes is for seven different values of V [$N \tilde{=}$ no shots for each value of V; the error bar in $\bar{n}$ is $\sigma/(N-1)^{\frac{1}{2}}$, σ = standard deviation].

The occurrence of restrikes on the electrodes is affected by the value of L_o. The purpose of these measurements was also to find the influence of restrikes behind the first current sheath on the axial-focus stage of this first sheath. The analysis of our data indicates that the correlation coefficient α_1 for n vs. ν (ν = number of sharp peaks in the $|\dot{I}|$ signal from one discharge $\nu \tilde{=}$ 1-10) is negative ($\alpha_1 = -0.45$) for low voltage discharges ($V \tilde{=} 14$ kV, number of discharges about 50; the probability of non-significant random effects as a cause of this value of α_1 is < 0.1); $\alpha_1 \tilde{\tilde{=}} 0$ (no correlation) for intermediate voltages ($15 \leq V < 17$ kV); $\alpha_1 \tilde{\tilde{=}} 0.4$ (positive correlation) for a higher voltage ($V \geq 18$ kV); a similar behavior was observed in the correlation coefficients for n vs. $\Sigma \dot{H}_i$, n vs. ΣH_i^2, n vs. $\Sigma H_i \Delta_i$ (where H_i is the maximum value of the i-th peak in $|\dot{I}|$ and Δ_i is the FWHM of this peak). For all discharges at 17.5 kV a more detailed analysis was carried out. The steepness of the rise of the $|\dot{I}|$ signal vs. time was evaluated for the first peak of $|\dot{I}|$ in a time interval from 150 ns before the $|\dot{I}|$ peak to peak

time t=0 ($|\dot{I}|$ was fitted with $A\tilde{\tau}^{\gamma}$, $\tilde{\tau} = [t(ns) + 150)/150]$. The value of γ fitting best between 50 and 10 ns before the peak was derived for a group of high yield discharges, $n \geq 3\bar{n}$, with a mean value $\bar{\gamma} = 4.5$ and for the group of all the other discharges ($0.1\ \bar{n} < n \leq 1.5\ \bar{n}$) with a mean value $\bar{\gamma} = 3.9$. This result is considered as significant. The area ΔI_1 under the first $|\dot{I}|$ peak was also numerically estimated for these two groups of 17.5 kV discharges; ΔI_1 for the high-yield discharges (15% of all discharges at 17.5 kV) has the largest mean value; the ratio of the mean values of ΔI_1 of the two groups is = 8.5/6.5.

Low yield discharges have $|\dot{I}|$ signals which frequently indicates occurrence of restrikes at late times. A conclusion of these measurements is that in order to have a high yield discharge at a relatively low voltage (and low speed of the current sheath) the production of a small number of electron beams corresponds to the optimization of the system. At a high voltage the reverse is true (the production of many beams seems to help in avoiding restrikes and to avoid the formation at a late time, $\tilde{\sim}$ 1 μs, after the first discharge on the insulator, of another current sheath behind the first sheath).

6. Conclusions

The data in Table I indicate that the electron distribution as a function of energy - in the electrom beam which is ejected along the electrode axis (backward /180^{0} direction) - is consistent with the ion distribution reported in Fig. 5 for the ions ejected in the forward (i.e. 0^{0}) direction. The ion spectrum varies from shot to shot but specific features as in Fig. 5 are observed by all discharges. A peak at the same energy (300-400 keV) for both electron and ion spectra fits a particle acceleration process in which the same field accelerates both ions and electrons. X-ray and neutron-emission measurements with collimators indicate (Ref. 1, 2 and Ref. quoted therein) that ion beams and electron beams are generated in the same localized volume ($\sim$1 cm long) in the axial region of the discharge.

An important contribution to this research work at Stevens Institute was given by J. Feugeas, H. Kilic and C. Powell.

Fig. 1. Schematic view of plasma focus system (electrodes, vacuum system and electron-beam drift chamber), target and Rogowski coil locations.

Fig. 2. Dendrites in PMMA. The dendrites are produced by target exposure to a single discharge. The electron beam penetrates the PMMA target in the direction orthogonal to the target surface (target surface orthogonal to paper) as the arrow indicates.

Fig. 3. Typical oscilloscope signals (Tektronix 7844) for the electron beam current $\dot{I}_e$ (upper trace) and for the electrode current $\dot{I}$ (time derivatives). Discharge in 3 torr of D_2; the same gas and pressure was in the electron beam drift chamber (12.5 V/cm upper trace; 10 V/cm lower trace). Total neutron in the discharge 2×10^8. The number of peaks in the electron beam current, usually fits the number of peak, in the electrode current signal.

Fig. 4. Total neutron yield/per discharge as a function of applied voltage on the electrodes (the error bar indicates the standard deviation). The total inductance of the external circuit (capacitor bank, switches, transmission lines and electrodes) to obtain this set of data was increased to $L_o \overset{\sim}{} 60$ nh (usual value < 40 nh).

Fig. 5. Energy spectrum of the ion beam ejected by one plasma focus discharge in the axial forward direction (0^o); the experiment and the method (A) of derivation for this spectrum have been extensively reported in two publications, (1), (5) which have been listed at page 2 of this report.

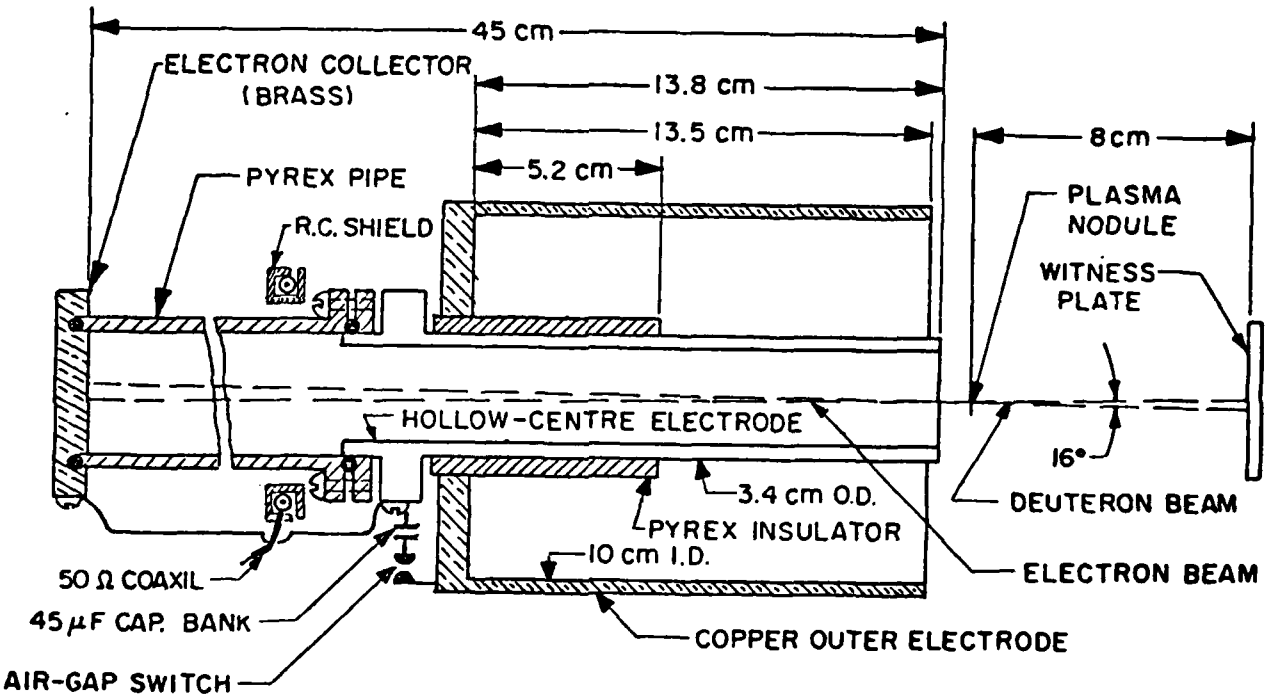
45 cm
ELECTRON COLLECTOR
(BRASS)
13.8 cm
13.5 cm
8cm
5.2 cm
PYREX PIPE
R.C. SHIELD
PLASMA
NODULE
WITNESS
PLATE
HOLLOW-CENTRE ELECTRODE
16°
3.4 cm O.D.
DEUTERON BEAM
PYREX INSULATOR
10 cm I.D.
50 Ω COAXIL
ELECTRON BEAM
45 μF CAP. BANK
COPPER OUTER ELECTRODE
AIR-GAP SWITCH

Fig. 1

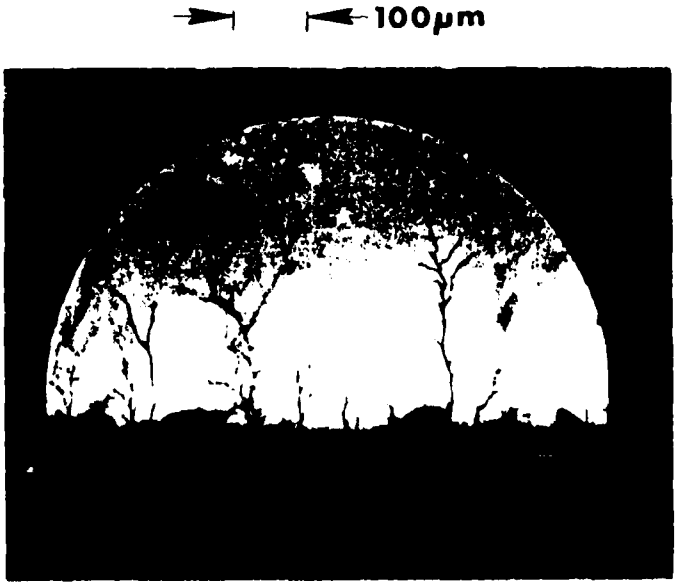

Fig. 2

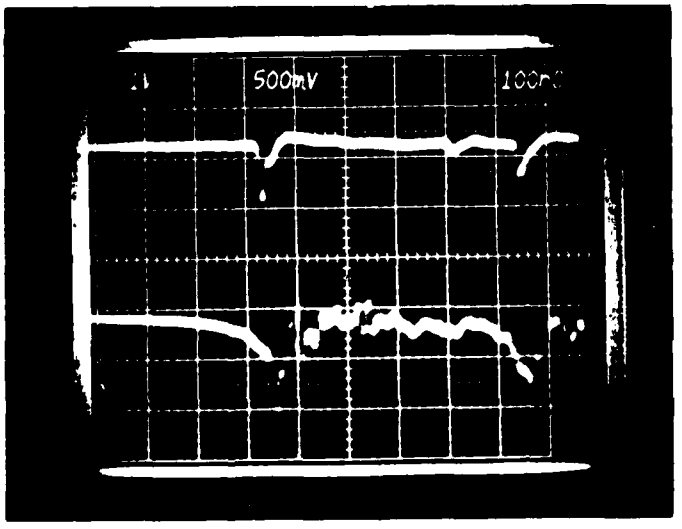

Fig. 3

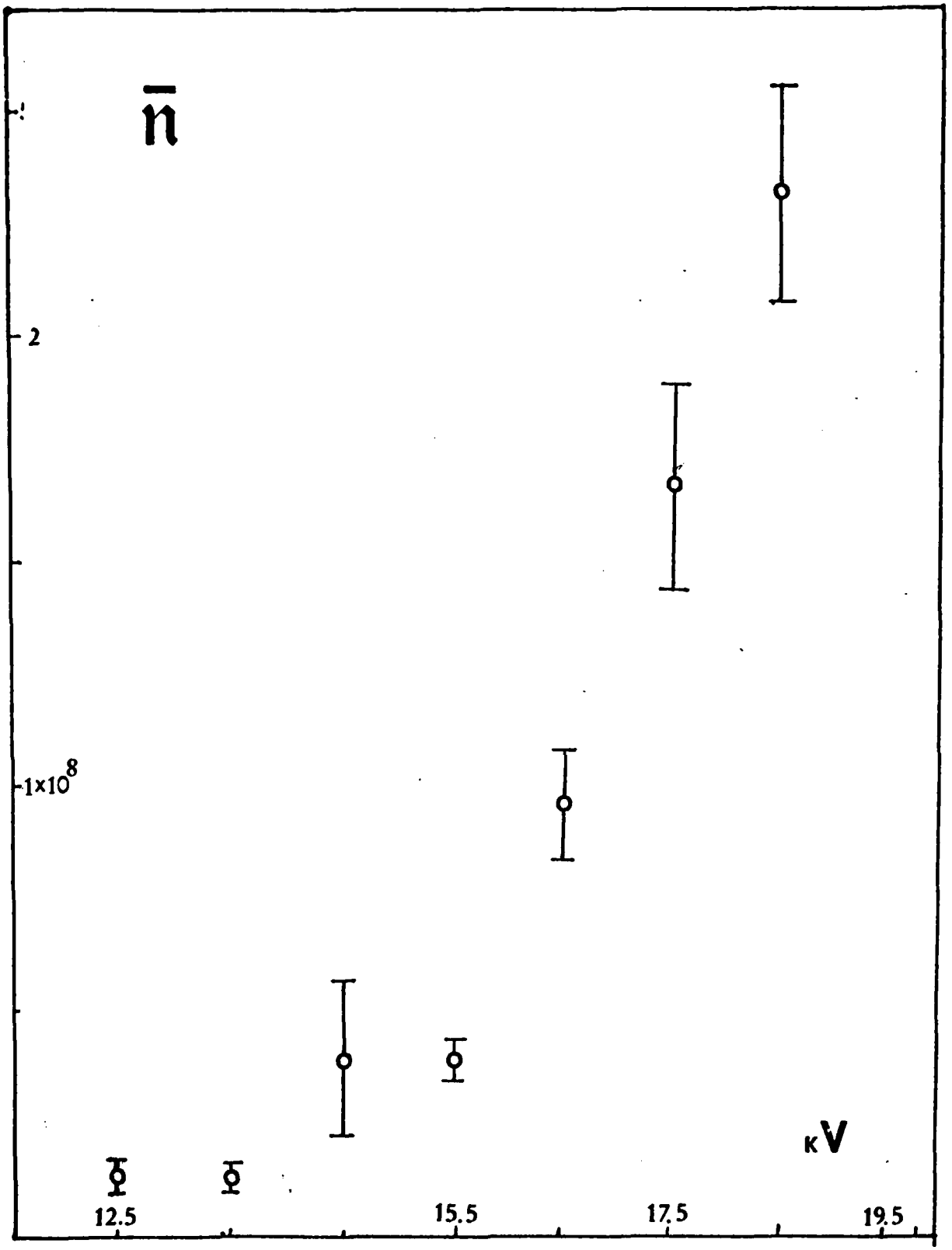

Fig. 4

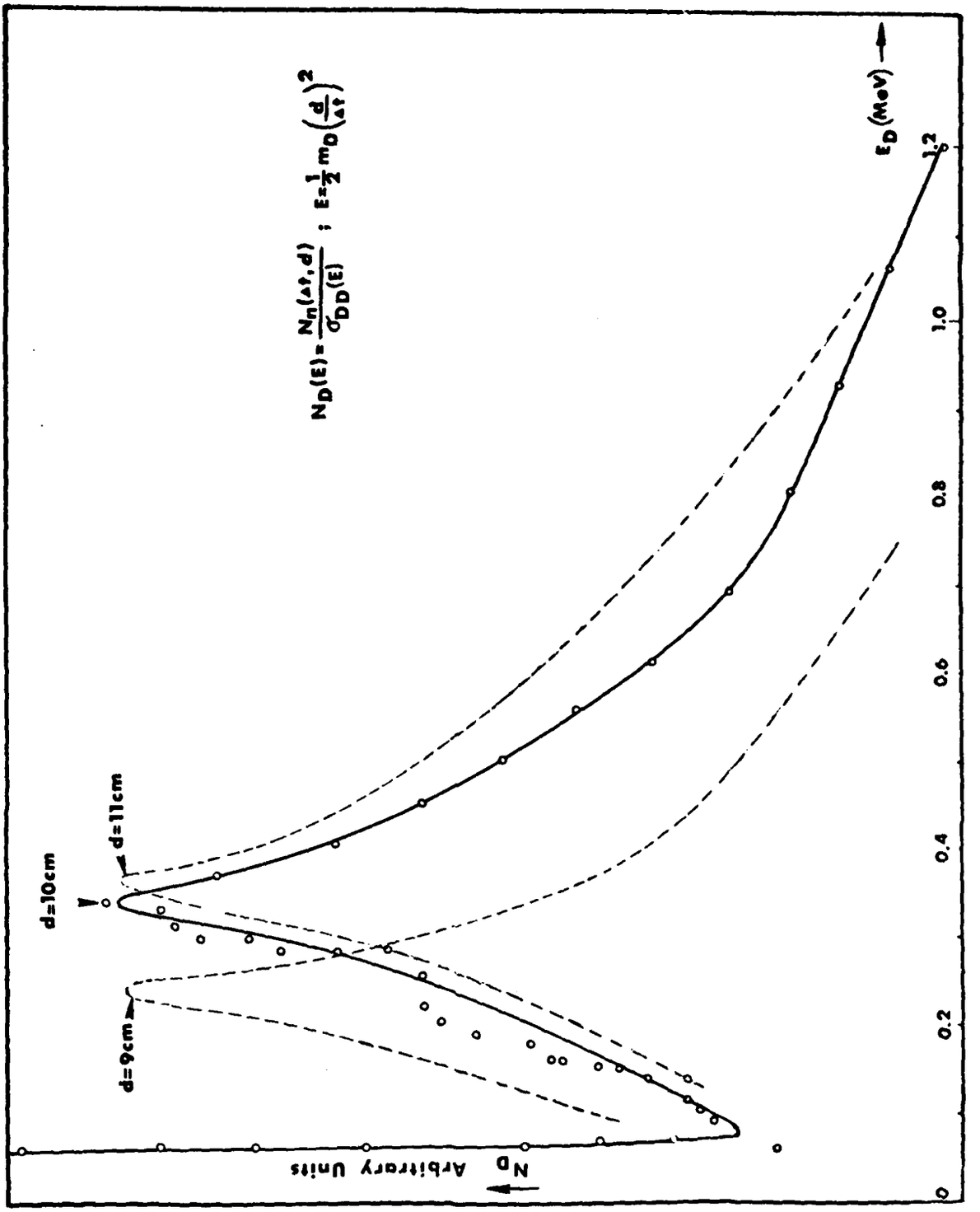
$N_D(E) = \frac{N_n(\Delta t, d)}{\sigma_{DD}(E)}$; $E = \frac{1}{2} m_D \left(\frac{d}{\Delta t}\right)^2$
E_D (MeV)
0
0.2
0.4
0.6
0.8
1.0
1.2
N_D Arbitrary Units
d=10cm
d=11cm
d=9cm

Fig. 5

References

(1). Bostick, Nardi, Prior: Nucl. Fusion Conf., Berchtesgaden 1976, (IAEA) Vol. 3, p. 497.

(2). Bostick, et al: Energy Storage Compression and Switching, 1976 (Plenum) p. 261.

(3). Bostick, Nardi, Prior, J. Plasma Physics 1972, Vol. 8, p. 7.

(4). Bostick, et al: J. Nuclear Material 1976, Vol. 63, p. 356.

(5). Spencer L. V.: Nat. Bureau of Standards, Monograph 1 (Sept. 10, 1959).
Molen, G. M.: Aerospace Corp. Report, April 8, 1976.
Bostick, Nardi, Prior, Opt. Soc. of Am. Technical Digest, Feb. 1978, p. Th 21-25.

(6). Gross B. J.: Polymer Science, Vol. XXVII, p. 138 (1958).

(7). Berger M. J., Seltzer S. M. : "Tables of Energy Losses and Ranges of Electrons and Positrons", U.S. Dept. of Commerce, N65-12606 (1964).

(8). Lackner H.: J. Applied Physics, Vol. 36, 6 (June 1965).

(9). O'Dwyer J. J.: Theory of Dielectric Breakdown of Solids, Oxford, 1964,p.111.

(10). Furuta J., Hiraoka E., Okamoto S.: J. Appl. Physics 37, 1873 (1966).

(11). Nardi V.: Proc. 2nd Topical Conf. on Pulsed High-Beta Plasmas, Garching 1972, Lotz Edit., p. 163.

(12). Bostick, Nardi, Prior: Nucl. Fusion Conf., Tokyo, 1974 (IEAE), Vol. 3, p. 109.